Pressure dependence of the $BaFe_2As_2$ Fermi surface within the spin density wave state

D. Graf,[1] R. Stillwell,[1] T. P. Murphy,[1] J.-H. Park,[1] E. C. Palm,[1] P. Schlottmann,[1,2] R. D. McDonald,[3] J. G. Analytis,[4,5] I. R. Fisher,[4,5] and S. W. Tozer[1]

[1]*National High Magnetic Field Laboratory, Florida State University, Tallahassee, Florida 32310, USA*

[2]*Department of Physics, Florida State University, Tallahassee, Florida 32306, USA*

[3]*Los Alamos National Laboratory, Los Alamos, New Mexico 87545, USA*

[4]*Geballe Laboratory for Advanced Materials and Department of Applied Physics, Stanford University, Stanford, California 94305, USA*

[5]*Stanford Institute for Materials and Energy Sciences, SLAC National Accelerator Laboratory, 2575 Sand Hill Road, Menlo Park, California 94025, USA*

(Received 11 November 2011; revised manuscript received 9 March 2012; published 3 April 2012)

Measuring surface conductivity we have observed the evolution of Shubnikov de Haas oscillations under quasihydrostatic pressure for the pnictide parent compound $BaFe_2As_2$. Prior results in the reconstructed state have observed small pockets which emerge from zone folding as a result of structural changes with cooling. For pressures below 20 kbar, both Fermi surface orbits grow in size. The effective masses increase with pressure suggesting enhanced correlation in the system, and a series of magnetic breakdown orbits are observed confirming that band structure calculations setting them in close proximity are correct.

DOI: 10.1103/PhysRevB.85.134503 PACS number(s): 72.15.Gd, 74.62.Fj, 74.70.Xa

I. INTRODUCTION

The iron arsenide compounds have created excitement in recent years as part of a new generation of high transition temperature materials. One of the keys to developing a better understanding of the nature of superconductivity in these compounds is to determine the effect of varying experimental parameters, such as magnetic field, temperature, and pressure. With cooling, $BaFe_2As_2$ concurrently undergoes both structural and magnetic transitions.[1] At room temperature, the $ThCr_2Si_2$-type tetragonal structure is found before ordering at $T \sim 140$ K to an orthorhombic structure. Antiferromagnetic ordering of the Fe moments lead to a spin density wave (SDW) state[2] which is not fully gapped, allowing for the observation of the Fermi surface. Band structure calculations based on the high temperature, nonmagnetic structure of $BaFe_2As_2$ predict quasi-two-dimensional closed orbits,[3] but the Fermi surface is reconstructed as the Brillioun zone is folded, leaving small, unnested pockets.

Measurements of the Fermi surface of AFe_2As_2 (A = Ba,Ca,and Sr) by surface conductivity and magnetization have shown small orbits from the remaining Fermi surface, where each orbit is less than 2% of the first Brillioun zone.[4–6] All of these measurements have taken advantage of pulsed magnetic fields where the maximum fields exceed 60 T. This allowed for analysis of a larger number of quantum oscillation peaks from the low frequency orbits where most orbits were not resolved in fields below 20 T. Here we present results of the Fermi surface of $BaFe_2As_2$ at ambient and applied pressure measured by surface conductivity in dc fields. The high quality of the single crystals used is demonstrated by the observation of quantum oscillations at ambient pressure in fields as low as 3.5 T [see Fig. 1(a)].

The effect of chemical and applied pressure has been explored extensively in this family of materials. The compound becomes a superconductor by doping each of the elemental components of $BaFe_2As_2$ with K (20%, $T_c \sim 25$ K), Co (8%, $T_c \sim 22$ K), or P (33%, $T_c \sim 31$ K), respectively.[7–9] Initial superconducting quantum interference device (SQUID) magnetization data at pressures of ∼27 kbar showed superconductivity in the undoped parent compound.[10] Subsequent resistivity measurements to above 100 kbar using a cubic anvil cell did not reveal any zero resistivity results[11,12] and showed the SDW state persists to ∼80 kbar, emphasizing the importance of hydrostatic pressure media for these materials. The superconducting state in the Ca analogue was found using an oil medium with pressures as low as a few kilobar. However, using the hydrostatic conditions from a He gas pressure medium suppressed superconductivity.[13,14] The effect of applied pressure on the Fermi surface of the parent compounds to this point has been an open question.

II. EXPERIMENTAL DETAILS

An annealing procedure very similar to the one outlined in Ref. 4 was used before our measurements. The quality of the crystals is shown by a residual resistance ratio (RRR) of ∼23 for the resistance measurement shown in Fig. 1(d). Recently, small uniaxial strain applied along the b axis has been used to reveal the effect of crystal twinning that occurs at the structural transition within the ab plane.[15,16] The temperature dependence shows the clear signature of a twinned crystal. The RRR value is reasonable for the observation of quantum oscillations and a factor of 3 improvement over lower RRR values for $SrFe_2As_2$ where the Fermi surface was still resolved.[5] Numerous crystals were used in this study, but all samples went through the same annealing cycle before measurement and were cleaved from larger crystals in the same batch.

Diamond anvil cells (DACs) and piston cylinder cells (PCCs) were used for the measurements under pressure. The small DAC has a diameter of only 11.4 mm, with a similar length, allowing for full rotation within the diameter of the magnet bore. Nonmetallic gaskets[17] roughly ∼150 μm thick were placed between the 1.2 mm diameter diamond culets. Thin (∼12 μm) Cu wire was wrapped into coils of 10 to 40 turns, which were nested into a hole in the center of the gasket. The coil is soldered to a thin, flexible 0.7 mm coaxial

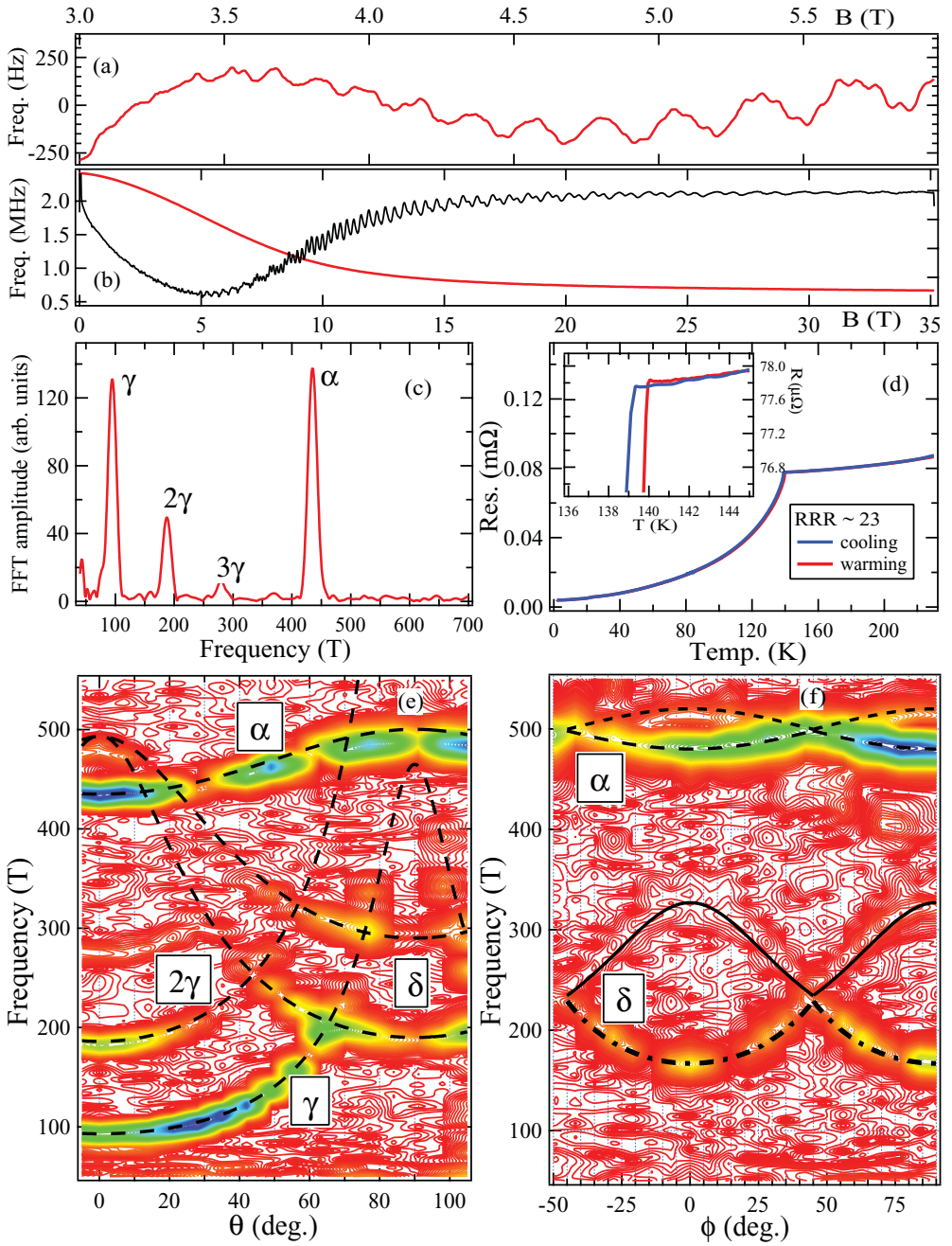

FIG. 1. (Color online) (a) Quantum oscillations are observed in surface conductivity at fields as low as ∼3.5 T with $T \sim 30$ mK and $B \| c$ axis. The background was subtracted from the data using a three term polynomial. (b) The TDO circuit frequency change from a field sweep ($T \sim 350$ mK) to 35 T (red/light) and the first derivative (black/dark) which clearly shows the quantum oscillations. (c) FFT spectrum for ambient pressure results. (d) Cooling and warming curve for 4-probe resistance showing evidence of twinning. The inset shows a more detailed view. The ∼0.5 K separation between cooling (2 K/min) and warming (0.5 K/min) curves reflects a lag in temperature response during cooling and is not intrinsic to the sample. (e) Contour plot of the frequencies from angular dependence taken from $\theta = 0^\circ$ ($B \| c$ axis) to $\theta = 90^\circ$ ($B \| ab$ plane). Dashed lines arefit to $F(\theta) \sim F_0/\{\cos^2(\theta) + [(1/\eta)\sin(\theta)]^2\}^{0.5}$, where $\eta =$ (major/minor) axis for the ellipsoid. (f) Contour plot of the frequencies from angular dependence taken with field aligned in the ab plane showing the four-fold symmetry created by twinning. The long dashed and dot-dashed lines are fits to the same form as (e). The solid and short dashed lines are fits to oblate ellipsoids where the ratio of major/minor axes is inverted.

cable which is connected to a tunnel diode oscillator (TDO) circuit board. When biased, the tank circuit resonates with frequencies of ∼10 to 50 MHz, depending on the circuit components, including the inductance of the sample coil. Changes in sample surface conductivity are observed as shifts in the frequency of the circuit. By taking care to maximize the filling factor of the sample within the coil and the number of coil windings within the cell gasket, a stable frequency with ∼1 to 10 ppm noise can be established. The PCC is setup similarly but the increased sample volume allows for larger

diameter coils of ∼50 to 100 turns. The length of the PCC (∼45 mm) did not allow for rotation within the available space in the magnet bore. Measurements were taken in two systems: a ^{3}He system positioned inside a 35 T resistive magnet and a dilution refrigerator in a 16 T superconducting magnet with base temperatures of ∼400 and 30 mK, respectively. Both are located at the National High Magnetic Field Laboratory in Tallahassee, Florida. The pressure cells were immersed directly into the liquid/gas for maximum thermal contact, and the temperature was measured using a calibrated Cernox thermometer ∼15 mm from the sample.

A single crystal was cleaved and centered in the coil with the c axis of the sample aligned with the axis of the coil. Measurements were made using pressure mediums of perfluorinated polyether fluid (oil), a 1:1 mixture of Fluorinert FC-70 and 77, and a 4:1 mixture of methanol and ethanol. Pressure was calibrated at room temperature and then again at low temperature ($T \sim 4$ K) using the shift of the ruby R1 fluorescence peak[18] in comparison with an ambient ruby at the same temperature. During the course of this work, hydrostaticity was estimated by two methods. First, the signal-to-noise ratio (SNR) of the results was examined by comparing the quantum oscillation amplitudes (∼0.1–10 kHz) and noise level, which was tens of hertz or below in most measurements. Second, the deviation of the full width half maximum (FWHM, hereafter Γ) of the R1 ruby peak from the ambient pressure value [$\Delta\Gamma = \Gamma(P) - \Gamma(0)$, where $\Gamma(0) \sim 0.090$ nm][19] can be used as a marker of increasing nonhydrostatic conditions. The data with the best SNR at high pressures was observed using a 1:1 mixture of fluorinert FC-70 and 77 in a PCC with a large sample volume. In the instances where $\Delta\Gamma > 0.1$, the amplitude of the quantum oscillations diminished too quickly at higher temperatures to fit effective masses, though the frequency of the fast Fourier transform peaks did not shift with different hydrostaticity conditions. The effective masses reported (Fig. 3) were the result of measurements with $\Delta\Gamma < 0.1$. The data with the best SNR in a DAC was found using a 4:1 methanol-ethanol mixture with a cooling rate of ∼1 to 2 K/min, which has been shown to maintain hydrostatic conditions to above 90 kbar.[20]

It is interesting to note that Duncan *et al.*[21] used three different pressure mediums (Daphne 7373 oil, a pentane-isopentane mixture, and steatite powder) to measure the effect on the SDW state of $BaFe_2As_2$. The results show that $BaFe_2As_2$ is highly susceptible to uniaxial strain causing a reduction of the c/a ratio and a suppression of the SDW state. The importance of the c/a ratio is also demonstrated through the de Haas van Alphen (dHvA) results of Analytis *et al.* of $SrFe_2P_2$ which show quasi-two-dimensional orbits and a nonmagnetic ground state, quite different from the arsenide analog.[22] The effect of annealing was explored on the Sr arsenide compound by Kirshenbaum *et al.*, where they found that superconductivity was suppressed by heat treatment but was enhanced by mechanical stress.[23]

III. RESULTS AND DISCUSSION

High resolution Shubnikov de Haas (SdH) oscillations observed at ambient pressure [Figs. 1(a), 1(b), and 1(e)] match well to the results found from measurements in pulsed magnetic fields. As mentioned above, the samples were annealed, but no special care was taken in regards to detwinning the samples to allow for comparison between ambient and pressure results from the same initial conditions. A fast Fourier transform [Fig. 1(c)] of a field sweep for $B \parallel c$ axis ($\theta = 0^\circ$) reveals a low frequency γ with a second and third harmonic as well as a larger, almost spherical, ellipsoidal orbit α. Though initial high field measurements seemed to indicate a second low frequency β with $F_0 \sim 180$ T, our findings show the orbit is the second harmonic of the γ frequency, in agreement with Ref. 24. Measurements in pulsed fields for $CaFe_2As_2$ also failed to observe a β orbit,[6] making it likely that a new study of the third parent compound, $SrFe_2As_2$, would reveal the same case. Further confirmation on the absence of a β orbit is shown by the pressure dependence of the frequency, which follows twice that of the γ orbit (further details below).

The γ orbit at ambient pressure is slightly larger than previously reported with a frequency of $F_\gamma \sim 93$ T. The ellipticity of the angular dependence was fit using $F(\theta) \sim F_0/\{[\cos(\theta)]^2 + [(1/\eta)\sin(\theta)]^2\}^{1/2}$ over a range of ∼110°, taken every ∼7° at $T \sim 400$ mK in fields up to 35 T. A value of $\eta \sim 5$ confirms the "cigar-shape" of the Fermi surface [Fig. 1(e)]. This result deviates slightly from the γ orbit of $CaFe_2As_2$ where the limited angular dependence is similar to the α orbit.[6] The third harmonic of the γ orbit is clearly visible with a minimum frequency of ∼273 T. The largest ellipsoidal surface has a frequency minimum of 433 T with $\eta \sim 1.15$, matching previous work. Effective masses of $0.74m_e$ and $1.35m_e$ were found for the γ and α orbits, respectively, in agreement within the error bars of the values in Ref. 4. Dingle temperatures of 2.2 and 2.7 K were determined from the γ and α orbits.

As the crystal is rotated away from $B \parallel c$ axis towards the ab plane, a third orbit δemerges for $\theta >$ ∼40°, where $\theta = 90^\circ$ corresponds to $\phi \sim -25^\circ$ in Fig. 1(f). The orbit is an oblate ellipsoid with larger cross section when B is along the c axis, as reported in Ref. 24. Figure 1(f) shows a composite set of FFTs for field sweeps taken in the ab plane where $\phi = 0^\circ$ has been defined at an angle of minimum/maximum frequency, but could relate to either the a or b orthorhombic axis. With the c axis symmetry of the α and γ pockets, twinning effects are not observed with rotation near the $B \parallel c$ axis orientation [Fig. 1(e)], but angular dependence within the ab plane clearly shows the result of twinning. As pointed out in Ref. 25, the structural transition creates domains which are offset ∼45° from the orthorhombic lattice. Figure 1(f) shows the α orbit with a weak prolate ellipsoid anisotropy which repeats after 90° (long dashed lines). The same orbit is observed with lower intensity orthogonal to this orbit (short dashed lines) with oblate angular dependence. The δ orbit is observed with a frequency of ∼170 T (330 T) with a prolate (oblate) angular dependence which also has a four-fold symmetry for rotation in the ab plane. The γ pocket, even if it is a closed three-dimensional (3D) ellipsoid, does not appear for measurements near the $B \parallel ab$ plane orientation. This could be due to end points that are not well resolved in the $\pm k_z$ directions, so the cross section of the orbit is not well defined.[26] The frequency peaks $F_\alpha \sim 480$ T and $F_\delta \sim 170$ T were found to have masses of $m^*_\alpha \sim 1.7m_e$ and $m^*_\delta \sim 1.0m_e$. The effective masses measured were consistently lower than those found in

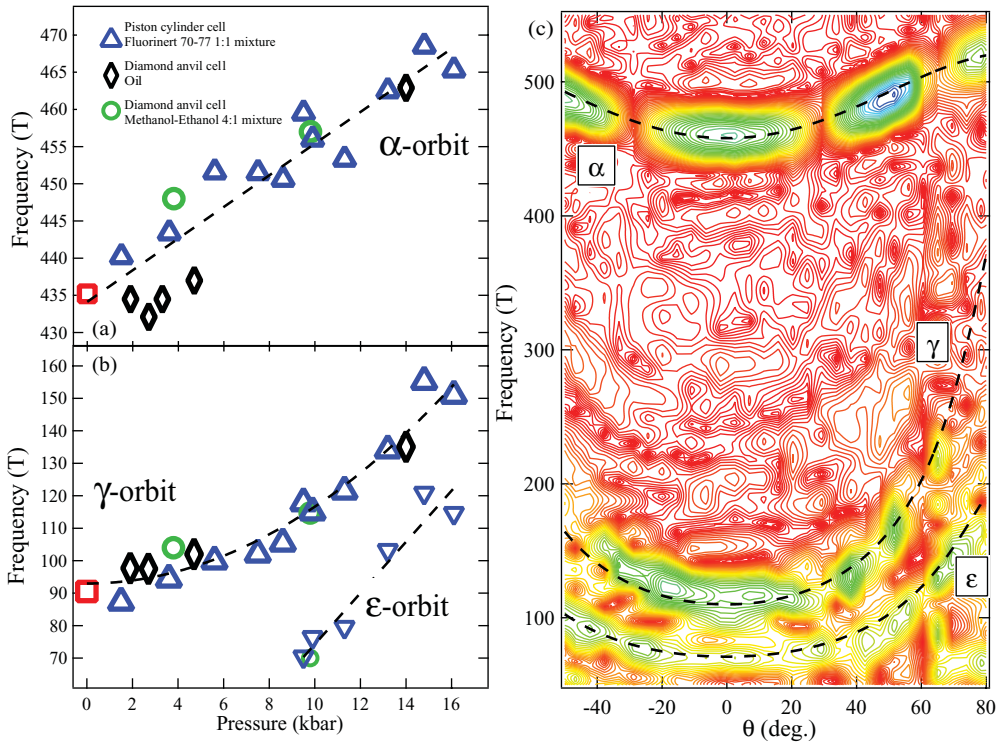

FIG. 2. (Color online) (a) Linear pressure dependence of the α orbit. (b) The γ orbit grows with increasing applied pressure up to ~16 kbar where a P^2 dependence of $(P) \sim 91 + 0.24P^2$ is found. Different pressure techniques and conditions are shown as symbols in the figure with red squares indicating the ambient pressure value. Pressure dependence of the ε orbit is also shown (see text for discussion). (c) Angular dependence of the FFTs taken at $P \sim 10$ kbar.

Ref. 24. These discrepancies could originate from decreased correlations in the larger magnetic fields used for the present measurements.

Using the Onsager relation[27] $A_k \sim F2\pi e/\hbar$, the γ and α pockets change from 0.3 and 1.7% of the first Brillioun zone at ambient pressure, respectively, to 0.7 and 1.8% at a pressure of ~16.1 kbar, with the magnetic field along the c axis. The smaller pocket increases much more dramatically and the different Fermi surface topologies display different types of pressure dependence. The nearly spherical α orbit has an increase in orbital frequency [Fig. 2(a)] with applied pressure that fits linearly with a slope of $\Delta F/\Delta P \sim 2.2$ T/kbar. The relationship between chemical and applied pressure is found in Ref. 28 where optimal phosphorus doping ($x \sim 0.33$) in $BaFe_2(As_{1-x}P_x)_2$ has the same superconducting transition temperature as the undoped compound at ~52 kbar. Using an estimate of ~1.6 kbar $\approx x = 0.01$ of phosphorus doping the linear pressure dependence of the α orbit would lead to $F \sim 550$ T at optimal doping. For a comparison, the doping dependence of the fermiology for $0.41 < x < 1$ is shown in Ref. 29, where quasi-two-dimensional orbits (labeled α and β) are found to have larger size with increasing x (i.e., "pressure"). Also, recent angle-resolved photoemission spectroscopy (ARPES) measurements[30] of $Ba(Fe_{1-x}Co_x)_2As_2$ suggest that the small holelike orbit, similar to the γ orbit, disappears in a Lifshitz transition for $x > 0.034$. If any chemical pressure is provided by the Co doping it seems to show the opposite effect [see Fig. 2(b)] as the applied pressure data shown in this report. The effect of applied pressure and electron doping with Co were explored by Ahilan *et al.*,[31] where T_{SDW} suppression and T_c enhancement were found with increasing pressure or with Co doping but a direct correlation between the two remains an open question.

The angular dependence of $BaFe_2As_2$ in a DAC was studied at a pressure of 10 kbar using a 4:1 mixture of methanol-ethanol as a pressure medium [Fig. 2(c)]. Though the frequency of the α orbit increases with pressure, the ellipticity of the orbit remains the same. The γ orbit is found to have an ellipticity of $\eta \sim 4$ at 10 kbar with $F_\gamma \sim 115$ T, showing the long, thin pocket becomes shorter and has an increasing belly with pressure. The δ orbit appears to be suppressed by strain and is not visible in data taken with the field aligned with the ab plane under pressure.

Beginning with pressures near 10 kbar, an additional small orbit appears near $F \sim 70$ T. Band structure calculations[4] suggest that two prolate ellipsoids exist at ambient pressure. Initially, one of them was assigned the designation of the β orbit which has since been shown to be the second harmonic of the γ orbit. As the angular dependence data of Fig. 2(c) shows, the ε pocket behaves similarly to γ suggesting that ε might be the second calculated cigar-shaped pocket. The angular dependence of this orbit shows $F_\varepsilon \sim 68$ T and $\eta \sim 2.7$. Another possible origin follows from the local spin density approximation approach used in Ref. 24 which shows an additional very small pocket, but the calculation was shifted for a better fit to observed orbits, making this assignment unlikely. Several points should be made about efforts to clarify this peak in the FFT. The ε orbit has been observed in several different

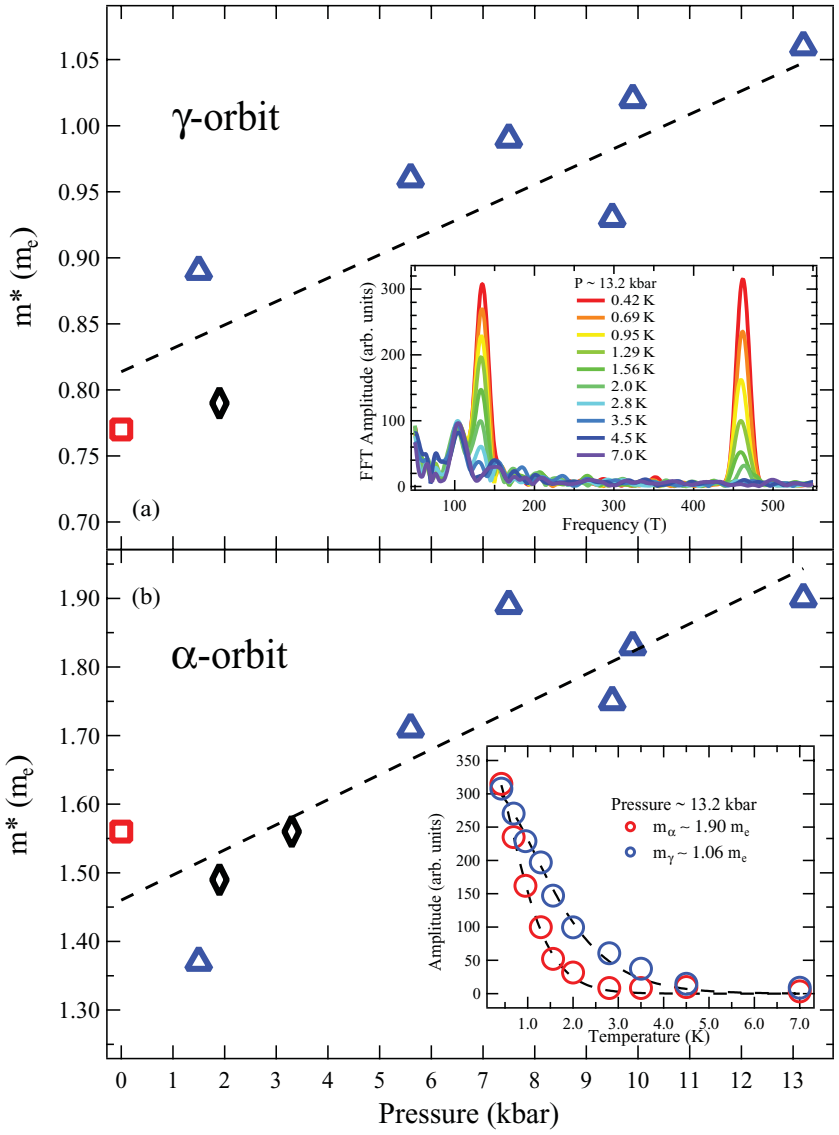

FIG. 3. (Color online) Pressure dependence of the effective masses for the (a) γ orbit and (b) α orbit at $\theta = 0^\circ$. Upper inset: temperature dependence to 7.0 K for $P \sim 13.2$ kbar. The symbols follow the same convention as Fig. 2. Lower inset: Effective mass fit (dashed lines) to the temperature dependence. The sizes of the markers correspond to error size taken from the noise floor of the FFTs.

samples under different applied pressures [see Fig. 2(b)]. Several different polynomial background subtractions were used as well as different levels of interpolation, but the peak only shifts frequency location slightly ($\sim\pm 10$ T). While the temperature dependence of this frequency has been resolved to temperatures as high as 7 K, no decrease in FFT amplitude is clearly observed. A possible source of this behavior is an orbit resulting from a Dirac cone which would produce a very light mass as has been suggested in Ref. 32. In the cases when this orbit was observed in the Fourier spectrum, the frequency has been included on Fig. 2(a). Further work to higher pressures is planned to shed more light on this portion of the Fermi surface.

The effective masses were measured with the magnetic field aligned with the c axis of the crystals, giving the smallest cross section of the thin γ orbit. With increasing pressure, the effective masses of the α and γ orbits both grow slightly larger, as shown in Fig. 3. The inset to Fig. 3(a) shows the temperature dependence of the FFT at a pressure of 13.2 kbar while the inset to Fig. 3(b) shows the effective mass fitting using the temperature damping factor $R_T = X/\sinh(X)$ (Ref. 33). The mass of the γ orbit grows at $\Delta m^*/\Delta P \sim 0.018 m_e$/kbar while the larger mass of the α orbit grows nearly twice as fast with $\Delta m^*/\Delta P \sim 0.035 m_e$/kbar. As found by the dHvA measurements of Shishido,[29] the effective mass of the β orbit of $BaFe_2(As_{1-x}P_x)_2$ appears to grow at an increasing rate as x approaches the optimal value in the superconducting state ($x \sim 0.33$), which is most likely due to stronger many body interactions. In addition, a change was observed in the power law of the temperature dependence ($r \propto T^n$) where Fermi liquid behavior ($n \sim 2$) begins to deviate towards $n \sim 1$ near optimal doping.[34] Further, NMR studies[35] of the ^{31}P nucleus found a correlation between antiferromagnetic (AF) fluctuations and the enhancement of the effective mass found in Ref. 29 with P doping. These results along with the increase in mass (albeit gradual) with applied pressure shown here suggest a quantum critical point at the center of the superconducting state.

The fast Fourier transform amplitude is plotted on the log scale in Fig. 4(a) with the magnetic field along the c axis of the sample. An exponential decrease in peak amplitude of successive harmonics is observed following the expected behavior from the combined thermal and Dingle factors of the

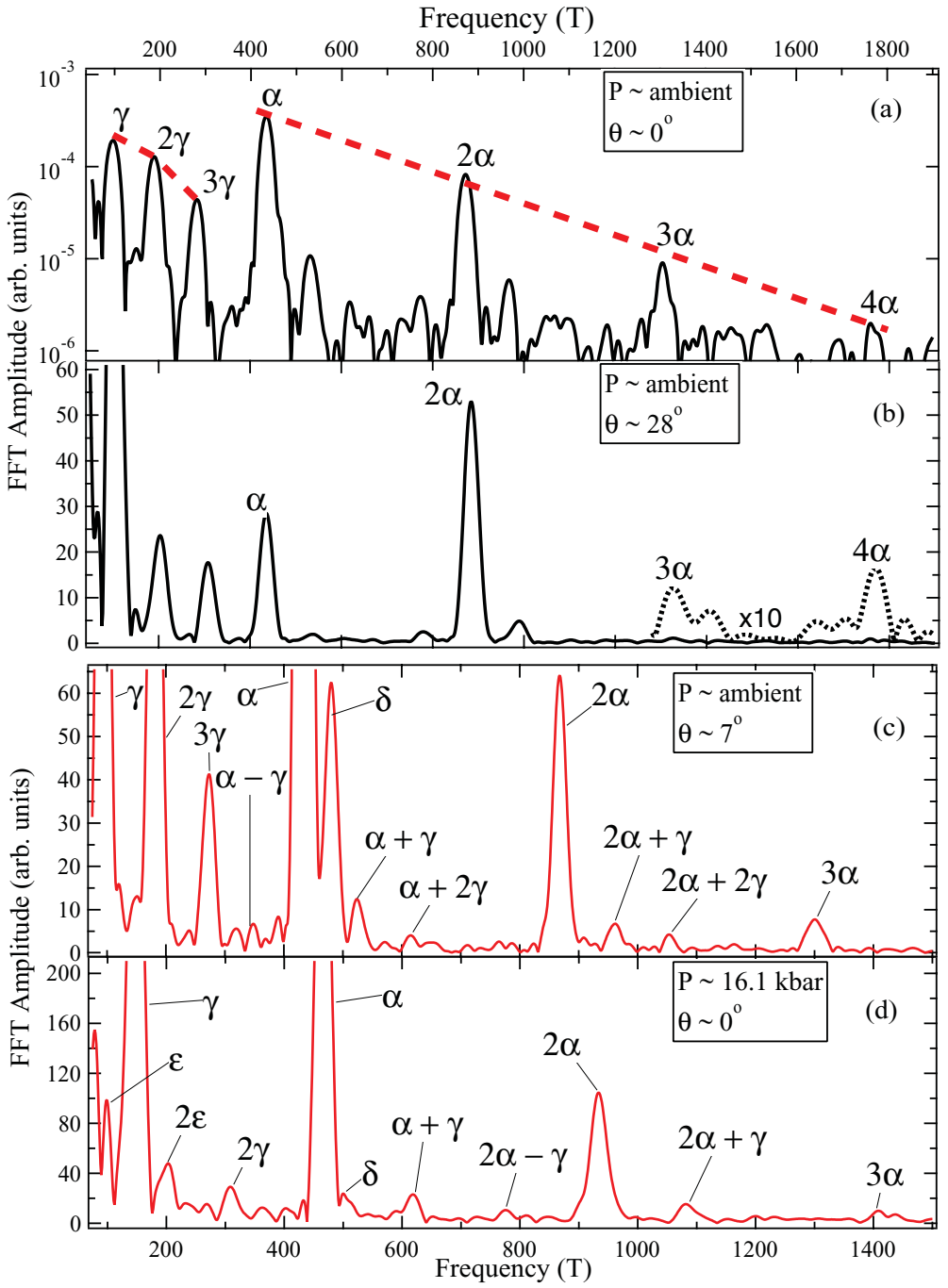

FIG. 4. (Color online) (a) Fourier spectrum of $BaFe_2As_2$ oscillations at ambient pressure and $\theta = 0^\circ$ orientation shown on a log scale. An exponential decay is observed for the peak amplitudes except the first harmonic for the γ orbit.[33] Red dashed lines are a guide to the eye. (b) Fourier spectrum at ambient pressure tilted $\sim 28^\circ$ away from the c axis where odd harmonics have been reduced by spin zeros. The Fourier spectrum showing the fundamental, harmonics, and combination frequencies shifted by pressure are shown at (c) ambient pressure and (d) pressure ~ 16.1 kbar. (c) and (d) have been expanded along the amplitude axis to show the harmonic and combination peaks more clearly. All measurements shown in (a) to (d) were taken at ~ 440 mK.

Lifshitz-Kosevich (LK) formula.[33] The FFT peak amplitudes for the α orbit show symmetric minima at orientations of $\theta \sim \pm 28^\circ$ and $\pm$ 63° (not shown). As shown by Figs. 1(e) and 2(c) and in agreement with Ref. 24, this effect occurs independent of pressure and at the same orientations, and originates from Zeeman splitting of the Landau levels. The LK parameter, $R_s = \cos(rg\mu\pi/2)$, describes this phenomenon (where g is the spin g factor, μ is the cyclotron mass normalized by the free electron mass, and r is the harmonic number). The superposition of spin-up and -down orbits in some orientations leads to a decrease in the amplitude of the odd harmonics compared to the even harmonics [Fig. 4(b)].

Figures 4(c) and 4(d) show the FFT of $BaFe_2As_2$ with and without applied pressure. Combination frequencies of the γ

and α orbits are found. Because of the rapid increase in the size of the γ orbit with applied pressure in comparison to the α orbit, at $P \sim 16.1$ kbar we find $F_\alpha \sim F_{3\gamma}$. Combination frequencies can occur for several reasons. Magnetic interaction between carriers can result in combination frequencies (Shoenberg effect) through a modified internal field which includes the full magnetic induction, rather than only the applied field.[27] Similarly, a charge-density or spin density wave order parameter can give rise to a nonlinear coupling of Fermi surface frequencies, i.e., frequency mixing.[36] It is difficult to differentiate this from magnetic breakdown, but the fact that the combination frequencies with summed orbits (i.e., $\alpha + \gamma$) consistently have a higher FFT amplitude suggests that the selection rules from magnetic breakdown may be the source of these frequencies. The band structure calculations shown in Ref. 4 and the SDW transition temperature ($T \sim 140$ K $\sim$ 12 meV) provide constraints for an estimate of the breakdown field. Assuming Fermi and gap energies of $E_F \sim 120$ meV and $E_g \sim 12$ meV, a breakdown field of $B_{MB} \sim (m^* E_g^2/\hbar e E_F) \sim 10$ T is found which is easily within experimental limits. This assumes that the α and γ orbits are in close enough proximity for this small gap.

In summary, we have made high resolution measurements of Shubnikov de Haas oscillations for $BaFe_2As_2$ at ambient and quasihydrostatic pressure. The small Fermi surface pockets previously reported grow dramatically with increased pressure, answering the question of the effect of applied pressure on the reconstructed Fermi surface. In addition, a small pocket ε is observed which may correlate with the Dirac cone found in APRES measurements. The effective masses grow with pressure in contrast to conventional metals such as sodium. In addition, we have confirmed how essential hydrostatic conditions are to the accurate measurement of this material. The quality of results improved moving from an oil-based medium with a lower hydrostatic limit to conventional Fluorinert and methanol-ethanol mixtures. Whether the pressure conditions necessary to recover the paramagnetic state can be met in a DAC is an open question for high field quantum oscillation measurements.

ACKNOWLEDGMENTS

This work was funded by the DOE/NNSA under Grant No. DE-FG52-10NA29659 and was performed at the National High Magnetic Field Laboratory which is supported by NSF Cooperative Agreement No. DMR-0654118 and by the State of Florida. P.S. is supported by the DOE under Grant No. DE-FG02-98ER45707. Work performed at Stanford University was supported by the Department of Energy, Office of Basic Energy Sciences, under Contract No. DE-AC02-76SF00515. We thank J. S. Brooks and S. Uji for useful discussions.

[1] Q. Huang, Y. Qiu, W. Bao, M. A. Green, J. W. Lynn, Y. C. Gasparovic, T. Wu, G. Wu, and X. H. Chen, Phys. Rev. Lett. **101**, 257003 (2008).

[2] C. Krellner, N. Caroca-Canales, A. Jesche, H. Rosner, A. Ormeci, and C. Geibel, Phys. Rev. B **78**, 100504 (2008).

[3] D. J. Singh, Phys. Rev. B **78**, 094511 (2008).

[4] J. G. Analytis, R. D. McDonald, J. H. Chu, S. C. Riggs, A. F. Bangura, C. Kucharczyk, M. Johannes, and I. R. Fisher, Phys. Rev. B **80**, 064507 (2009).

[5] S. E. Sebastian, J. Gillett, N. Harrison, P. H. C. Lau, D. J. Singh, C. H. Mielke, and G. G. Lonzarich, J. Phys. Condens. Matter **20**, 422203 (2008).

[6] N. Harrison, R. D. McDonald, C. H. Mielke, E. D. Bauer, F. Ronning, and J. D. Thompson, J. Phys. Condens. Matter **21**, 322202 (2009).

[7] M. Rotter, M. Pangerl, M. Tegel, and D. Johrendt, Angew. Chem., Int. Ed. **47**, 7949 (2008).

[8] A. S. Sefat, R. Y. Jin, M. A. McGuire, B. C. Sales, D. J. Singh, and D. Mandrus, Phys. Rev. Lett. **101**, 117004 (2008).

[9] S. Kasahara *et al.*, Phys. Rev. B **81**, 184519 (2010).

[10] P. L. Alireza, Y. T. C. Ko, J. Gillett, C. M. Petrone, J. M. Cole, G. G. Lonzarich, and S. E. Sebastian, J. Phys. Condens. Matter **21**, 012208 (2009).

[11] H. Fukazawa *et al.*, J. Phys. Soc. Jpn. **77**, 105004 (2008).

[12] K. Matsubayashi, N. Katayama, K. Ohgushi, A. Yamada, K. Munakata, T. Matsumoto, and Y. Uwatoko, J. Phys. Soc. Jpn. **78**, 073706 (2009).

[13] M. S. Torikachvili, S. L. Bud'ko, N. Ni, and P. C. Canfield, Phys. Rev. Lett. **101**, 057006 (2008).

[14] W. Yu, A. A. Aczel, T. J. Williams, S. L. Bud'ko, N. Ni, P. C. Canfield, and G. M. Luke, Phys. Rev. B **79**, 020511 (2009).

[15] J.-H. Chu, J. G. Analytis, K. D. Greve, P. L. McMahon, Z. Islam, Y. Yamamoto, and I. R. Fisher, Science **329**, 824 (2010).

[16] I. R. Fisher, L. Degiorgi, and Z. X. Shen, Rep. Prog. Phys. **74**, 124506 (2011).

[17] D. Graf, R. L. Stillwell, K. M. Purcell, and S. W. Tozer, High Press. Res. **31**, 533 (2011).

[18] G. J. Piermarini, S. Block, J. D. Barnett, and R. A. Forman, J. Appl. Phys. **46**, 2774 (1975).

[19] N. Tateiwa and Y. Haga, Rev. Sci. Instrum. **80**, 123901 (2009).

[20] R. J. Angel, M. Bujak, J. Zhao, G. D. Gatta, and S. D. Jacobsen, J. Appl. Crystallogr. **40**, 26 (2007).

[21] W. J. Duncan, O. P. Welzel, C. Harrison, X. F. Wang, X. H. Chen, F. M. Grosche, and P. G. Niklowitz, J. Phys. Condens. Matter **22**, 052201 (2010).

[22] J. G. Analytis, C. M. J. Andrew, A. I. Coldea, A. McCollam, J. H. Chu, R. D. McDonald, I. R. Fisher, and A. Carrington, Phys. Rev. Lett. **103**, 076401 (2009).

[23] K. C. Kirshenbaum, S. R. Saha, N. P. Butch, J. D. Magill, and J. Paglione, in *Science and Technology for Humanity (TIC-STH), 2009 IEEE Toronto International Conference* (IEEE, New York, 2009), p. 861.

[24] T. Terashima *et al.*, Phys. Rev. Lett. **107**, 176402 (2011).

[25] M. A. Tanatar, A. Kreyssig, S. Nandi, N. Ni, S. L. Bud'ko, P. C. Canfield, A. I. Goldman, and R. Prozorov, Phys. Rev. B **79**, 180508 (2009).

[26] N. Harrison and S. E. Sebastian, Phys. Rev. B **80**, 224512 (2009).

[27]D. Shoenberg, *Magnetic Oscillations in Metals* (Cambridge University Press, Cambridge, England, 1984).
[28]L. E. Klintberg, S. K. Goh, S. Kasahara, Y. Nakai, K. Ishida, M. Sutherland, T. Shibauchi, Y. Matsuda, and T. Terashima, J. Phys. Soc. Jpn. **79**, 123706 (2010).
[29]H. Shishido *et al.*, Phys. Rev. Lett. **104**, 057008 (2010).
[30]C. Liu *et al.*, Nat. Phys. **6**, 419 (2010).
[31]K. Ahilan, F. L. Ning, T. Imai, A. S. Sefat, M. A. McGuire, B. C. Sales, and D. Mandrus, Phys. Rev. B **79**, 214520 (2009).
[32]P. Richard *et al.*, Phys. Rev. Lett. **104**, 137001 (2010).
[33]The thermal damping factor, $R_T = X/\sinh(X)$ can be approximated by $\sim 2X\exp(-X)$ for sufficiently large $X = rm^*\kappa T/B$, where r = harmonic index, m^* = effective cyclotron mass, and $\kappa = 14.7\,\mathrm{T/K}$. The combination of R_T and the Dingle factor $R_D = \exp(-rm^*\kappa T_D/B)$ (where T_D is the Dingle temperature) account for the exponential decrease in the amplitude of the harmonics except for the $r = 1$ peak of the γ orbit where the $X/\sinh(X)$ term is used.
[34]A. Carrington, Rep. Prog. Phys. **74**, 124507 (2011).
[35]Y. Nakai *et al.*, Phys. Rev. Lett. **105**, 107003 (2010).
[36]P. Schlottmann and L. M. Falicov, Phys. Rev. Lett. **38**, 855 (1977).